

# The Characteristics of Graphene Obtained from Rice Husk and Graphite

M.A. Seitzhanova<sup>1,2,\*</sup>, Z.A. Mansurov<sup>2</sup>, M. Yeleuov<sup>2</sup>, V. Roviello<sup>3</sup>, R. Di Capua<sup>4</sup>

<sup>1</sup>Al-Farabi Kazakh National University, 050038 al-Farabi ave. 71, Almaty, Kazakhstan

<sup>2</sup>Institute of Combustion Problems, 050012, Bogenbay batyr str. 172, Almaty, Kazakhstan

<sup>3</sup>Advanced Metrologic Service Center (CESMA), University of Naples Federico II, Naples, Italy

<sup>4</sup>Department of Physics, University of Naples Federico II, and CNR-SPIN, Naples, Italy

## Article info

*Received:*

20 December 2018

*Received in revised form:*

6 February 2019

*Accepted:*

27 March 2019

## Keywords

Graphene

Graphite

Rice husk

Carbonization

Chemical activation

## Abstract

In this paper a method for obtaining graphene oxide from rice husk were developed using an approach based on a four-stage strategy: preliminary carbonization, desilication, activation with KOH, and exfoliation and its comparison with the method of graphite oxidation. The samples were analyzed by SEM, TEM, Raman, TGA, FTIR and elemental analysis. The elemental analysis show that the proposed approach allows to produce graphene materials with the content of carbon of about 70% and rich in inorganic matter (0–20 wt.%) (K, Fe, Si). To remove inorganic contents, purification and functionalization step were applied. The Raman spectra of the samples indicate the presence of a mixture of graphene layers and amorphous carbon. The thermogravimetric profile of samples is characterized by a slowly weight decrease up to a final residue of ~10 wt.%. FTIR spectra are characterized by a typical broad shape of large condensed aromatic carbon bonds. The work novelty can be reported as one method, one method of chemical synthesis. The use of a natural precursor – rice husk makes this method very economical for large-scale production.

## 1. Introduction

Recently, graphene and graphene oxides (GO) have found independent use as materials for nano-electronics, component of polymer and inorganic composite materials, solar batteries, supercapacitors, membranes, adsorbents, quantum dots, fluorescent material for biology and medicine [1–4]. Graphene is a semimetal with overlap of the valence and the conduction bands (material with zero band-gap) [5]. Unlike the ideal graphene sheet, graphene oxides consist of a 2D mesh of bound carbon atoms in the sp<sup>2</sup> and sp<sup>3</sup> hybridization states. Most sp<sup>3</sup> hybridized carbon atoms in graphene oxides are covalently bounded with oxygen in the form of epoxy, hydroxyl, and carboxyl groups [6–12].

Synthesis of graphene (single layer of graphite) has been reported as early as in 1975 by B. Lang [13]. After several attempts by various sci-

entists, eventually Novoselov et al. received credit for the discovery of graphene in 2004 [14]. They presented a reproducible method for the synthesis of graphene by mechanical exfoliation, but this method is not suitable for large-scale production. There are other well-known methods also available for the synthesis of graphene, which are associated with a number of mechanical operations: mixing, spraying, impregnation [15]. In this regard, compared with the powder state of the substance, it is more convenient to use colloidal dispersions. Among the methods for obtaining colloidal dispersions of graphene oxide, chemical methods prevail. Moreover, the main advantages of chemical methods are the possibility of large-scale production of the product and the relative simplicity of its functionalization due to the presence of active oxygen-containing groups [16]. Currently, many researchers are trying to develop green synthesis processes for graphene production [17–18, 3]. The purpose of green synthesis methods is to use a natural precursor and not to use toxic chemicals.

\*Corresponding author. E-mail: makpal\_90.90@mail.ru

Despite such an extensive range of various uses of graphene and its oxides, graphite is the main source material for the synthesis of these substances. However, in nature there are other materials, the structure of which contains graphene layers, like rice husk (RH), which contains biogenic silica. Matos J. and coworkers detailed studied nanostructured carbon derived from rice husk and role of meso- and macropores for adsorption of nitrobenzene [19, 20]. Such materials could be a potential material basis for obtaining graphene oxides. The purpose of this work is to compare the characteristics of graphene obtained from rice husk and graphite.

## 2 Experimental

### 2.1. Materials and chemicals

Potassium hydroxide and sodium hydroxide were purchased from "LABHIMPROM" (Chemical Analytical Trading Company, Almaty, Kazakhstan) (TU 24363-80). Rice husk (RH) was delivered from Bakanas village, district center of Balkhash, Almaty region, Kazakhstan. Graphite was delivered from Russia. Hydrogen peroxide (37%) was purchased from "LABOR PHARMA" (Trade and Production Company, Almaty, Kazakhstan) (OST 301-02-206-99). Sodium nitrate (pure) was purchased from FIRMA SCAT (produced by Open Joint Stock Company "Reactiv", Russia) (GOST 4168-79). Potassium permanganate was purchased from a pharmacy.  $H_2SO_4$  (98 wt.%), Sodium chloride (chemical pure) was purchased from REACHEM (Chemical Reagents Company, Moscow, Russia) (TU 6-09-5417-88) and from "LABOR PHARMA" (Trade and Production Company, Almaty, Kazakhstan) (GOST 4233-77).

### 2.2. Synthesis and functionalization of graphene oxide

Graphene oxide (GO) was obtained from RH and graphite. The production of GO from rice husk was realized by adapting the top-down approach from carbonized rice husk (CRH) reported in [21]. Briefly, CRH was desilicated and then mixed with KOH (carbon to KOH ratio: 1:4 and 1:5) and activated in air medium at 850 °C for 2 h. After that, the material was washed with water until up to pH~7 was obtained, and dried at 105 °C. The yield was about 3 wt.%. To functionalize the samples, 0.3 g of each selected sample and 10 mL of 15M

$H_2SO_4$  were added in a round-bottom flask. The temperature was controlled at 80 °C. After stirring for 60 min or 24 h, the mixture was centrifuged for 10 min (4000 r/min), then the recovered solid was washed out with bidistilled water many times to reach pH~7 and filtrated with PVDF membrane. The resulted sample was dried at 105 °C for 12 h. The second method was developed using Robert Murray Smith method. Firstly, 5 g of graphite powder, 2.5 g of  $NaNO_3$ , and 115 mL of  $H_2SO_4$  were placed in a round-bottom flask simultaneously stirring the mixture for 30 min to get a homogeneous solution. The resulting mixture was put in ice bath and 15 g of  $KMnO_4$  were slowly added. After that, deionized water (230 mL) was added to this mixture and stirred for 15 min with a magnetic stirrer. Then,  $H_2O$  (400 mL) and  $H_2O_2$  (50 mL, 37%) were added to this solution and heated to 98 °C and sonicated for 1 h. The resulting solution was filtered through membrane (type MFAS – SPA) and washed several times with deionized water to reach neutral pH. The weight of the final product was 5 g.

### 2.3. Instrumental techniques

Elemental analysis was performed by using two different instruments: the PRIMACS100 analyzer (series SNACCESS Version 1.0.29.100) and the CHN 628 LECO elemental analyzer according to the ASTM E870 procedure using EDTA as standard. Two measurements were performed and the average values are determined for each sample (maximum relative error ~0.7%). Scanning Electron Microscopy (SEM) was performed using Nova NanoSem 450 FEI/ThermoFisher. The powders were deposited on an aluminium stub, Au, Pd coated and introduced into the specimen chamber of a field emission scanning electron microscope, at 3.00 kV in a high vacuum mode, using an Everhart Thornley Detector (ETD) and Through the Lens Detector (TLD) for detailed micrographs and elemental microanalysis (EDX) at 15.00 kV. Raman microspectroscopy was performed on a two different Raman microscopes (Solver Spectrum (NT-MDT) and Jasco, NRS-3100). By the first one, Raman spectra were obtained by excitation with a blue laser with a wavelength of 473 nm, the signal accumulation time was 30 sec. The spectral resolution of the grating is 4  $cm^{-1}$ . By the second one, the 514 nm water-cooled Ar + laser line with a power of 4 mW per sample was injected into an Olympus integrated microscope and focused to a spot diameter of approximately 2  $\mu m$  by a 100x lens.

A holographic notch filter was used to deflect the laser excitation line. The Raman measurements were performed at least three times for greater reproducibility. Cyclohexane was used for wavelength calibration. Infrared spectroscopy (FTIR) analysis of materials was performed on solid dispersions of samples obtained by mixing and grinding of powdered materials (0.5–0.8 wt.%) with KBr. Pellets of solid mixtures were obtained by pressing at 10 t for 10 min. FTIR spectra in the range of 3400–400  $\text{cm}^{-1}$  were obtained in transmission mode using the spectrophotometer Nicolet 5700. Proximate analysis and ash content evaluation were performed by using a TGA 701 LECO analyzer. The thermogravimetric data collected as a result of the thermal reaction are compiled into a graph of the mass or percentage of the initial mass on the y-axis versus the temperature or time on the x-axis. This graph, which is often smoothed, is called the TGA curve. The first derivative of the TGA curve can be constructed to determine inflection points useful for in-depth interpretation as well as for differential thermal analysis.

### 3. Results and discussion

The processes of pre-carbonization and carbonization were monitored by measuring the density, elemental composition, mechanical properties, and

the height of the carbon layer plane. Therefore, RH was pre-carbonized at 273–300 °C. The purpose of potassium hydroxide is therefore to provide both carbon retention (higher yields, e.g., less amount of volatiles are formed as hydrocarbon tar) and high surface area. In a general view, interaction between carbon and KOH starts with solid–solid reactions and then proceeds according to the reactions between solid and liquid, including the recovery of potassium compounds (K) with the formation of metal K, oxidation of carbon to oxide and carbonate, and other reactions among the different active intermediates [22]. The real reaction processes and activation mechanisms are variable depending not only on the activation parameters (i.e. amount of KOH, activation temperature, etc.), but also on the reactivity of various carbon sources. To determine the optimal conditions for obtaining graphene, several samples were analyzed. The main features of samples are given in Table 1.

The comparison between graphene oxide obtained from graphite and the graphene obtained by the activation of CRH indicates that they appear very similar as concerns structure, composition and basic properties. At the same time, the whole production process of obtaining graphene from graphite took no more than four hours, and the oxidation stage itself takes only 15 min, which is many times faster than when using activation methods.

**Table**  
The general characteristics of RH, CRH and graphene samples

Sample ID	Label	Preparation conditions	General characteristics	Size of samples by SEM analysis
Initial Rice Husk	RH	Not treated	Intact and not friable sample	Millimetric size
Precarbonized Rice Husk	CRH	Desilicated	Very friable sample	Millimetric size
Graphene (CRH:KOH = 1:4)	Gr(1/4) <sub>1</sub>	30 min desilicated, in air	Particles of similar dimension and friable aggregates	800-90 (many) $\mu\text{m}$ ; 40-4 (some small) $\mu\text{m}$
Graphene (CRH:KOH = 1:4)	Gr(1/4) <sub>2</sub>	60 min desilicated, in argon gas,	Very friable sample	Few 1 mm-300 $\mu\text{m}$ ; 70-3 (many) $\mu\text{m}$ and also very small (<3) $\mu\text{m}$
Graphene (CRH:KOH = 1:4)	Gr(1/4) <sub>3</sub>	Don't desilicated, exfoliated by $\text{H}_2\text{O}_2$	Particles as sheets very friable	900-200 (many) $\mu\text{m}$ ; 100-20 (some) $\mu\text{m}$ ; some very small (<10) $\mu\text{m}$
Graphene (CRH:KOH = 1:5)	Gr(1/5) <sub>1</sub>	Desilicated	Aggregates and very friable fragments	Some big 1,9 mm; 500-80 (many) $\mu\text{m}$ ; few very small (<10) $\mu\text{m}$
Graphene (CRH:KOH = 1:5)	Gr(1/5) <sub>2</sub>	Desilicated	Aggregates and very friable fragments	400-100 (many) $\mu\text{m}$ ; 20-2 (some) $\mu\text{m}$
Graphene oxide (Graphite)	GO	Oxidized, exfoliated by $\text{H}_2\text{O}_2$	Friable fragments	100-50 (many) $\mu\text{m}$ ; 20-2 (some) $\mu\text{m}$

### 3.1. Material composition

Carbonization at 850 °C coupled with chemical activation induces, as expected, the increase of carbon content and reduction of hydrogen content (Fig. 1).

As reported in Fig. 1, the samples Gr(1/4)<sub>3</sub> and GO exhibit the highest amount of carbon (75% and 88%), while the carbonized rice husk exhibits the lowest amount ~ 50%. It follows that the carbon contents increased with the increase in the amount of KOH. Accordingly, the hydrogen contents of samples decreased with the increase in the amount of KOH.

### 3.2. Thermogravimetric analysis

The thermogravimetric analysis allowed to estimate the ash content of selected samples. Even if the samples were burned at 800 °C in pure oxygen, a little amount of carbon was still present. Figure 2 reports some thermogravimetric profiles.

Raw RH is characterized by a significant weight loss at a temperature below 400 °C due to release of volatile components, then the weight decreases slowly and keeps constant up to a final residue of 15.5 wt.%. Similarly, the thermogravimetric profile of raw CRH is characterized by a weight loss

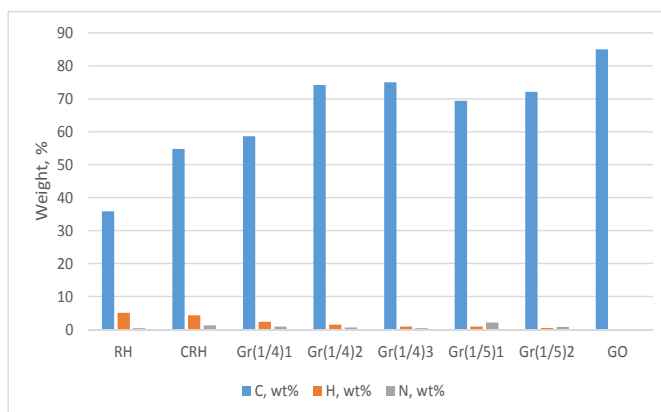


Fig. 1. The carbon, hydrogen and nitrogen contents of samples.

at a temperature below 400 °C release of volatile components, then the weight decreases slowly and keeps constant up to a final residue of 15.53 wt.%.

The thermogravimetric profile of raw Gr(1/4)<sub>2</sub> is characterized by a slowly weight decrease up to a final residue of 14.67 wt.%. The presence of a lower ash amount is indicative of a good purification process. The thermogravimetric profile of raw Gr(1/5)<sub>2</sub> is characterized by a slow weight decrease up to a final residue of 6.71 wt.%. It is worth to note the reddish color of the ashes. That color indicates the presence of some iron oxide from the walls of the crucible used for synthesis of samples.

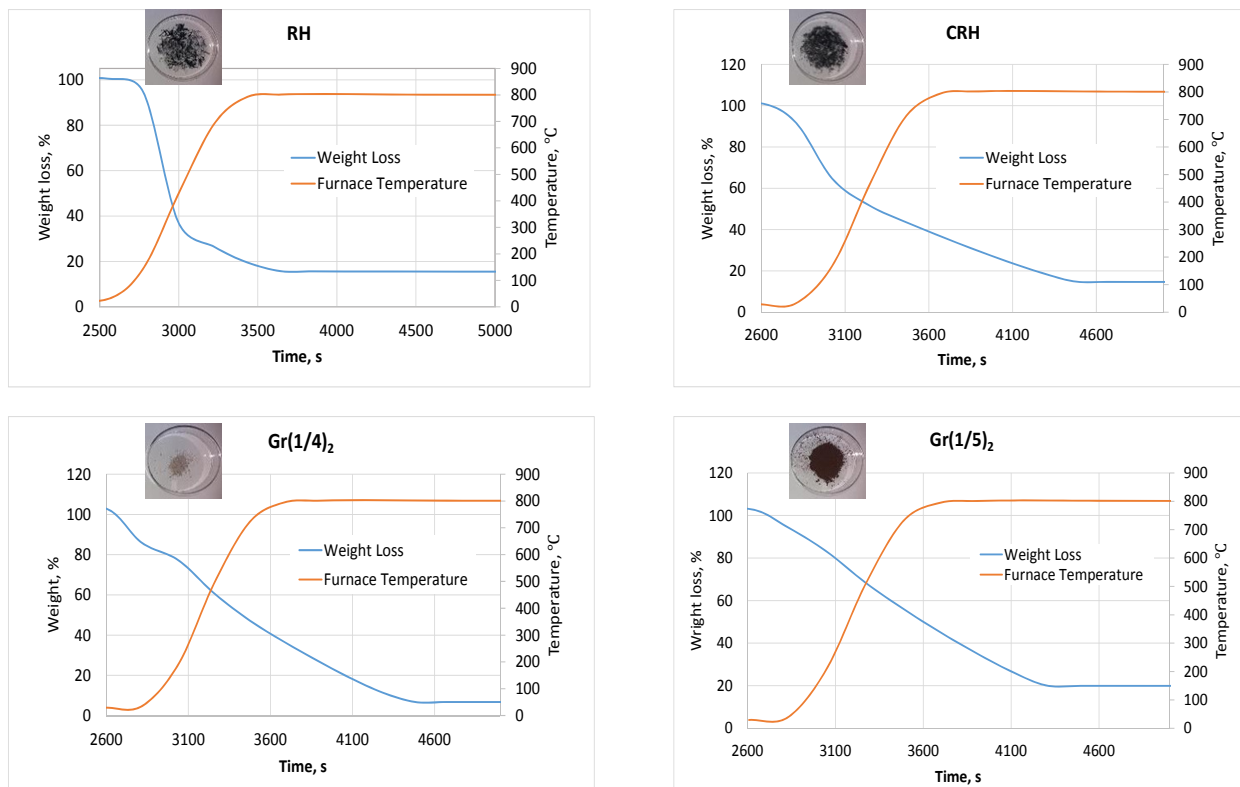


Fig. 2. TGA graphs on different samples (in the insets: images of ash).

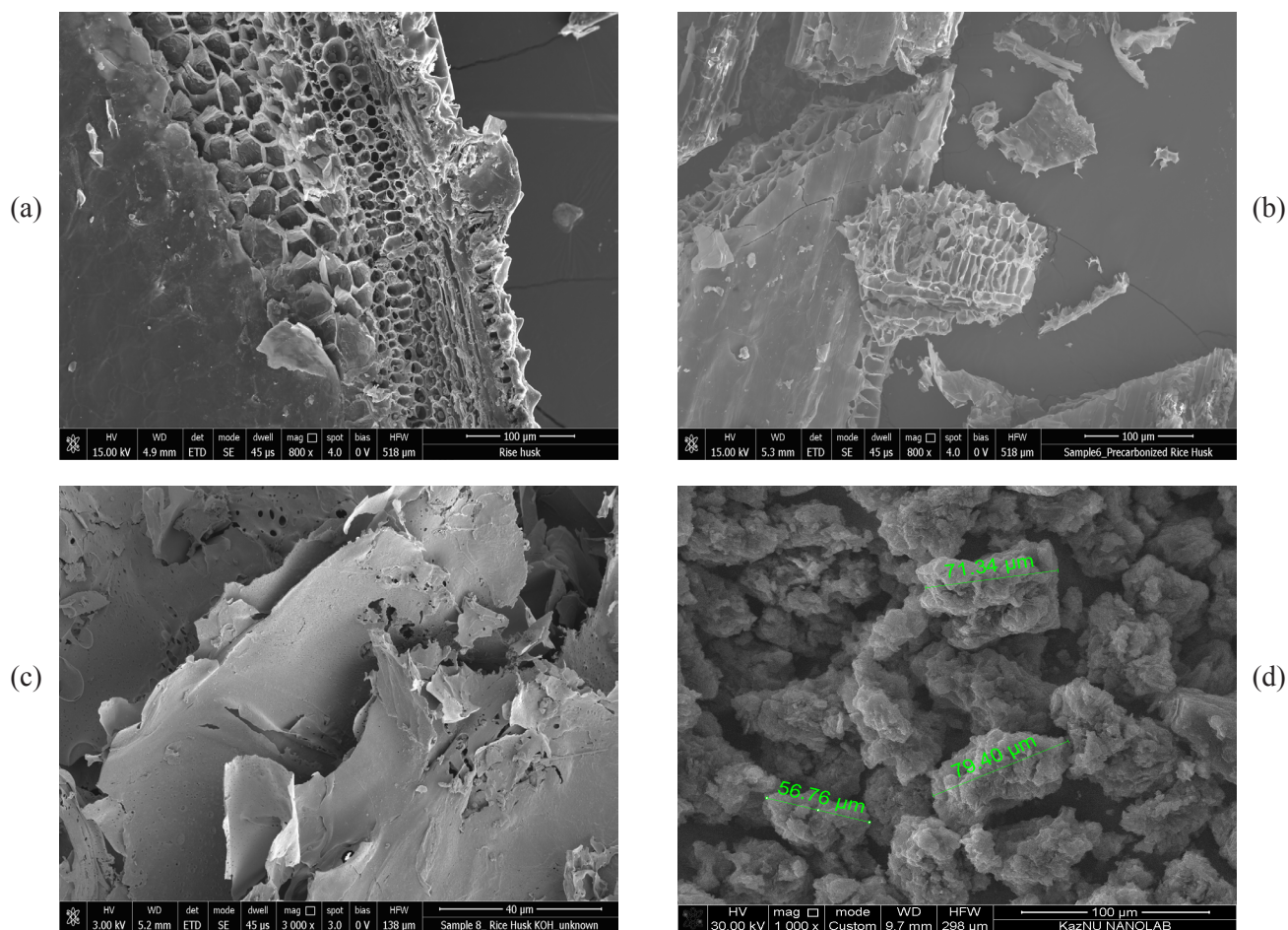


Fig. 3. Morphological characterization of the samples with different magnifications: (a) – RH; (b) – CRH, (c) – Gr(1/4)<sub>3</sub>; (d) – GO.

### 3.3. Morphology

The microscopic observations and microanalysis were performed to study the morphology of the raw RH, the CRH and Gr (obtained after activation with KOH in different ratios) and GO samples. SEM images of samples at different magnifications are shown in Fig. 3 (a)-(d). Figure 3 (a) shows the outer epidermis of rice husk, which is well organized and has a corrugated structure. The EDX analysis indicates that silica is mainly localized in a rigid layer of rice husk, and also fills the space between the epidermal cells. The silica concentration was high on the outer surfaces of the husk and much less on the inner surface and was virtually absent in the rice husk.

The SEM images of CRH (Fig. 3 (b)) show that many residual pores are distributed within the carbon sample, indicating that the pre-carbonized rice husk is a highly porous material with a large internal surface area. The rice husk broke up during thermal decomposition of organic matter. Although the result data did not show great

changes in its morphology compared to the initial rice husk, the SEM images show that the surface structure of the pre-carbonized rice husk changed significantly. The raw rice husk was intact and had a rather smooth surface, while the surface of CRH appeared to be uneven and exhibited cracks.

When CRH is activated with the chemical reagent KOH (1/4) at the temperature of 850 °C for 2 h, it gets exfoliated in CRH and the structure becomes more ordered (Fig. 3 (c)): the annealed graphene sheets acquire a layered structure throughout the cross section, continuing continuously in the longitudinal direction. However, during thermal annealing, micropores are formed making graphene sheets more porous.

The structure of the samples activated in the ratio of KOH 1/5 was found to be highly porous. A subsequent comparison of these samples with respect to the treatment conditions (activation at 850 °C and 2 h and 1/5 of CRH/KOH) shows a homogenous and uniform distribution of macropores and a greater size of pores. Probably, this effect depends on the interconnection of pores and

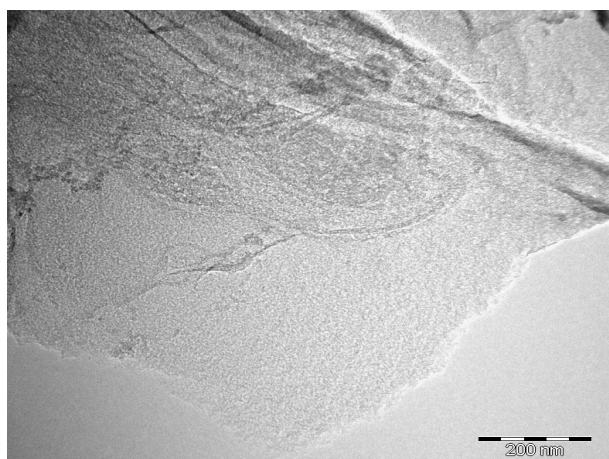


Fig. 4. TEM microimages of the graphene layers.

the treatment ratio of KOH. SEM imaging of GO (Fig. 3 (d)) clearly showed high degrees of agglomeration of graphene layers. The average size of GO layers  $\sim 70 \mu\text{m}$ .

Next, the structures of graphene layers were analyzed by transmission electron microscopy (TEM) using a JEM-2100 (JEOL, Japan) instrument with high stability of high voltage and beam current along with an excellent electron-optical system. A TEM image of graphene obtained from CRH by activation with KOH is shown in Fig. 4. Samples have defects and inclusions of an amorphous carbon component, but there are sections of layers without defects with a homogeneous surface structure.

### 3.4. Raman spectroscopy

Raman investigation was carried out to determine the presence of nanostructured 2D carbon, as graphene, and to estimate the number of layers characterizing the nanostructures. Raman investigation allows to distinguish amorphous carbon

from crystalline graphite or from graphene at different degrees of nanostructuring [23, 24]. The main features in the Raman spectra of carbon are the so-called peaks of G and D at the  $\sim 1560$  and  $1360 \text{ cm}^{-1}$ , respectively, for visible excitation. Non-amorphous  $\text{sp}^2$  carbon structures exhibit an additional G' (or 2D) band as well at  $2700 \text{ cm}^{-1}$ .

CRH exhibits some fluorescence, along with Raman features related to only amorphous carbon (D and G bands [25]), in all the treatments with no trace of G' band. According to the elemental analysis, two ( $\text{Gr}(1/5)_2$  and  $\text{Gr}(1/4)_3$ ) samples were analyzed in which the content of carbon was relatively high. The Raman spectra of these samples clearly indicate a mixture of amorphous and graphene entities. The ratio of the two components is spatially heterogeneous, so the spectra in Fig. 5 are only representative of the mixture of sample  $\text{Gr}(1/5)_1$  and  $\text{Gr}(1/4)_3$  (Fig. 5).

The both activated samples with ratio 1:4 ( $\text{Gr}(1/4)_3$ ) and 1:5 ( $\text{Gr}(1/5)_1$ ) exhibit D, G and G' bands. A significant spatial heterogeneity is detected, but two major components can be isolated: amorphous carbon (with D and G bands at  $1352$  and  $1594 \text{ cm}^{-1}$ ) and graphene (with detectable D, G and G' bands). The ratio  $I_{\text{G}}/I_{\text{G}'}$  was analyzed, only for those spots where amorphous carbon was considered negligible. For both samples  $\text{Gr}(1/5)_1$  and  $\text{Gr}(1/4)_3$ , the ratio  $I_{\text{G}}/I_{\text{G}'}$  is close to  $1.56 \pm 0.10$ , suggesting a multilayered structure.

Also, the sample obtained from graphite was analyzed by Raman spectroscopy. The results indicate a mixture of amorphous carbon and graphene entities, which corresponds to three peaks: peak D at  $1363 \text{ cm}^{-1}$ , peak G at  $1588 \text{ cm}^{-1}$ , and peak G' at  $2725 \text{ cm}^{-1}$  (Fig. 6).

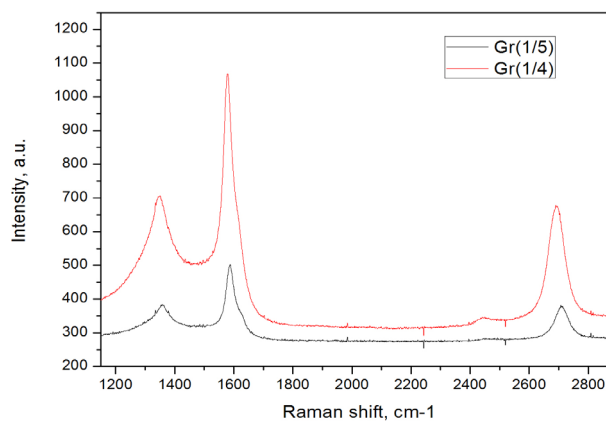


Fig. 5. Raman spectrum of the Gr samples obtained in different ratios of KOH

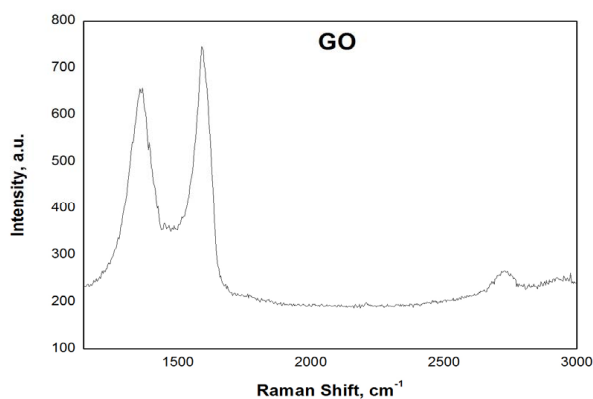


Fig. 6. Raman spectrum of the GO.

Nevertheless, all the Raman spectra showing G' bands exhibit very symmetric line shape, typical of a 1–2 layer graphene. Whatever is the number of layer (to be confirmed), the ratio and the lineshape suggest similar nanostructuring in samples Gr(1/5)<sub>1</sub> and Gr(1/4)<sub>3</sub>. Interestingly, in samples Gr(1/5)<sub>1</sub> and Gr(1/4)<sub>3</sub>, the graphene-related bands are somehow shifted: 1358/1596/2711 cm<sup>-1</sup> in sample Gr(1/4)<sub>3</sub>, and 1350/1579/2694 cm<sup>-1</sup> in sample Gr(1/5)<sub>1</sub>. By comparing sample Gr(1/5)<sub>1</sub> and Gr(1/4)<sub>3</sub> in the limited sampling performed, the activation ratio 1:5 provides a higher graphene content than 1:4. No effect functionalization of the samples with H<sub>2</sub>SO<sub>4</sub> was detected via Raman spectroscopy.

### 3.5. Fourier-transform infrared spectroscopy

Fourier-transform infrared spectroscopy (FTIR) analysis was performed on selected of samples: CRH, Gr(1/4)<sub>2</sub>, and Gr(1/5)<sub>1</sub>. The data are presented in Fig. 7.

CRH infrared spectrum is characterized by different contributions ascribable to various functional groups: ~ 3000 cm<sup>-1</sup>, low-intensity bands are due to the tensile vibrations of the aliphatic and aromatic bonds of C-H, and in the mid-frequency range (1700 and 1000 cm<sup>-1</sup>) a wide combination of peaks caused by the overlap of the carbon skeleton of the adsorption bands (C=O, C=C, C-C, C-H- C-O stretching and bending modes) was found [26]. Gr(1/4) and Gr(1/5) spectra are characterized by the typical broad shape of large condensed aromatic carbon networks. Only the peak due to C=C stretching modes and the overlapped peaks between 900 and 1500 cm<sup>-1</sup> due to skeleton vibrations are detected. The dc conductivities ( $\sigma$ ) of the solid sample dispersions prepared for FTIR measurements (0.5–0.8 wt.% in KBr) were:  $\sigma_{\text{CRH}} = 14 \pm 3$  nS/m,  $\sigma_{\text{Gr(1/4)}} = 80 \pm 10$  nS/m and  $\sigma_{\text{Gr(1/5)}} = 60 \pm 10$  nS/m. The dc conductivity

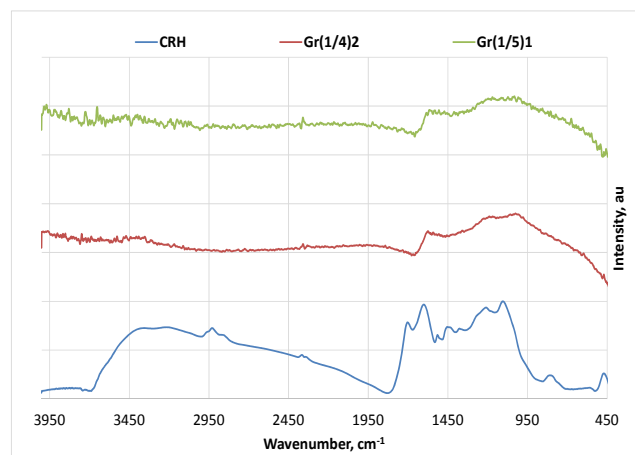


Fig. 7. FTIR spectrum of samples after washing and functionalization.

trend confirms that the more extended conductive moiety in the AC samples was stated. On the other hand, the sample on which the functionalization process was performed for 24 h is characterized by a main peak at 1090 cm<sup>-1</sup> due to sulfoxide groups.

## 4. Conclusions

A method of obtaining graphene from rice husk and graphite was developed. The carbonization/activation treatment of RH leads to the formation of a mixture of graphene layers and amorphous carbon. A higher amount of activation agent (1:5) seems to increase the relative amount of graphene component.

Intercalation of graphite powder with concentrated sulfuric acid is carried out, followed by oxidation under the influence of KMnO<sub>4</sub>, NaNO<sub>3</sub> and H<sub>2</sub>O<sub>2</sub>. It is shown that this method produces a complex mixture of flakes of different thickness. It has been established that direct dispersion of graphite cannot serve as a reliable method for obtaining significant quantities of graphene flakes with a small number of layers.

According to Raman spectroscopy, the CRH sample is amorphous, without the presence of graphene. Raman features of samples Gr(1/5)<sub>2</sub>, Gr(1/4)<sub>3</sub> and GO are similar and they have mixture of amorphous carbon and graphene. Graphene in samples Gr(1/5)<sub>2</sub> and Gr(1/4)<sub>3</sub> exhibits the same number of layers. The amount of graphene is higher in sample Gr(1/5)<sub>2</sub> than in sample Gr(1/4)<sub>3</sub>. By Raman spectroscopy, no effects of H<sub>2</sub>SO<sub>4</sub> treatment were detected.

FTIR results indicate that the functionalization during 1 h with H<sub>2</sub>SO<sub>4</sub> does not introduce significant change in the samples while that performed for 24 h successfully allowed the introduction of sulfonic groups.

## Acknowledgement

Authors would like to thank the National Nanotechnological Laboratory of Open Type of al-Farabi Kazakh National University and the “ACE” Laboratory of University of Naples Federico II, and Dr. Michela Alfè and Dr. Valentina Gargiulo of the Institute for Research on Combustion (IRC-CNR) (Naples, Italy) for their valuable guidance, and Prof. Alessandro Vergara (Department of Chemical Science at University of Naples, Italy) for assisting in Raman spectroscopy acquisition.

## References

- [1]. Z.A. Mansurov, Soot formation: textbook. Almaty: Kazakh University, 2015, 167 p.
- [2]. K.S. Novoselov, A.K. Geim, S.V. Dubonos, E.W. Hill, I.V. Grigorieva, *Nature* 426 (2003) 812–816. DOI: 10.1038/nature02180.
- [3]. H. Muramatsu, Y. Ahm Kim, K.-S. Yang, R. Cruz-Silva, I. Toda, T. Yamada, M. Terrones, M. Endo, T. Hayashi, H. Saitoh, *Small* 14 (2014) 2766–2770. DOI: 10.1002/smll.201400017
- [4]. J. Jao, L. Liu, F. Li Graphene Oxide: Physics and Applications. Berlin: Springer, 2015, p. 154.
- [5]. K.I. Ho, M. Boutchich; C.Y. Su, R. Moreddu, E. Marianathan, S.R. Eugene L. Montes, C.S. Lai, *Adv. Mater.* 27 (2015) 6519–6525. DOI: 10.1002/adma.201502544
- [6]. C. Berger, Z. Song, X. Li, X. Wu, N. Brown, C. Naud, D. Mayou, T. Li, J. Hass, A.N. Marchenkov, E.H. Conrad, P.N. First, W.A. de Heer, *Science* 312 (2006) 1191–1196. DOI: 10.1126/science.1125925
- [7]. M.S. Dresselhaus, P.T. Araujo, *ASC Nano* 4 (2010) 6297–6302. DOI: 10.1021/nn1029789
- [8]. D.P. Savitsky, A.S. Makarov, V.V. Goncharuk, *Dopov. Nac. akad. nauk Ukr.* 6 (2016) 87–94. DOI: 10.15407/dopovidi2016.06.087
- [9]. M.A. Rafiee, J. Rafiee, Z. Wang, H. Song, Z.-Z. Yu, N. Koratkar, *ACS Nano*, 3 (2009) 3884–3890. DOI: 10.1021/nn9010472.
- [10]. X. Zhao, Q. Zhang, D. Chen, P. Lu *Macromolecules* 43 (2010) 2357–2363. DOI: 10.1021/ma902862u
- [11]. I.W. Frank, D.M. Tanenbaum, A.M. van der Zande, P.L. McEuen, *J. Vac. Sci. Technol. B* 25 (2007) 2558–2561. DOI: 10.1116/1.2789446
- [12]. K. Min, N.R. Aluru, *Appl. Phys. Lett.* 98 (2011) 13111–13113. DOI: 10.1063/1.3534787.
- [13]. B. Lang, *Surf. Sci.* 53 (1975) 317–329. DOI: 10.1016/0039-6028(75)90132-6.
- [14]. K.S. Novoselov, A.K. Geim, S.V. Morozov, D. Jiang, Y. Zhang, S.V. Dubonos, I.V. Grigorieva, A.A. Firsov, *Science* 306 (2004) 666–669 DOI: 10.1126/science.1102896.
- [15]. N.G. Prikhod'ko, Z.A. Mansurov, M. Auelkhankyzy, B.T. Lesbayev, M. Nazhipkyzy, G.T. Smagulova, *Russ. J. Phys. Chem.* 9 (2015) 743–747. DOI: 10.1134/S1990793115050115
- [16]. E.D. Grayfer, V.G. Makotchenko, A.S. Nazarov, S.J. Kim, V.E. Fedorova, *Russ. Chem. Rev.* 80 (2011) 751–770. DOI: 10.1070/RC2011v080n08ABEH004181
- [17]. C. Zhu, S. Guo, Y. Fang, S. Dong, *ACS Nano*, 4 (2010) 2429–2437. DOI: 10.1021/nn1002387
- [18]. E. Ruiz-Hitzky, M. Darder, F.M. Fernandes, E. Zatile, F.J. Palomares, P. Aranda, *ADV. Mater.* 23 (2011) 5250–5255. DOI: 10.1002/adma.201101988.
- [19]. A. Dasgupta, J. Matos, H. Muramatsu, Y. Ono, V. Gonzalez, H. Liu, C. Rotella, K. Fujisawa, R. Cruz-Silva, Y. Hashimoto, M. Endo, K. Kaneko, L.R. Radovic, M. Terrones, *Carbon* 139 (2018) 833–844. DOI: 10.1016/j.carbon.2018.07.045
- [20]. M.C. Fernández de Cordoba, J. Matos, R. Montaña, P.S. Poon, S. Lanfredi, F.R. Praxedes, J.C. Hernández-Garrido, J.J. Calvino, E. Rodríguez-Aguado, E. Rodríguez-Castellón, C.O. Ania, *Catal. Today* 328 (2019) 125–135. DOI: 10.1016/j.cattod.2018.12.008
- [21]. M.A. Seitzhanova, D.I. Chenchik, Z.A. Mansurov, R. Di Capua, *Functional Nanostructures Proceedings* 1 (2017) 6–8.
- [22]. J.M. Jandosov, S.V. Mikhalovsky, C.A. Howell, D.I. Chenchik, B.K. Kosher, S.B. Lyubchik, J. Silvestre-Albero, N.T. Ablaihanova, G.T. Srailova, S.T. Tuleukhanov, S.V. Mikhalovsky, *Eurasian Chem. Tech. J.* 19 (2017) 303–313. DOI: 10.18321/ectj678
- [23]. A.C. Ferrari, J.C. Meyer, V. Scardaci, C. Casiraghi, M. Lazzeri, F. Mauri, S. Piscanec, D. Jiang, K.S. Novoselov, S. Roth, A.K. Geim, *Phys. Rev. Lett.* 97 (2006) 187401. DOI: 10.1103/PhysRevLett.97.187401
- [24]. J. Kaur, A. Vergara, M. Rossi, A.M. Gravagnuolo, M. Valadan, F. Corrado, M. Conte, F. Gesuele, P. Giardina, C. Altucci, *RSC Advances* 7 (2017) 50166–50175. DOI: 10.1039/C7RA09878B
- [25]. M. Alfè, V. Gargiulo, R. Di Capua, F. Chiarella, J.N. Rouzaud, A. Vergara, A. Ciajolo, *ACS Appl. Mater. Interfaces* 4 (2012) 4491–4498. DOI: 10.1021/am301197q
- [26]. R.M. Silverstein, F.X. Webster, D.J. Kiemle, 4th ed. Wiley, 2008.